HHS Public Access

Author manuscript

ACS Chem Biol. Author manuscript; available in PMC 2016 November 20.

Published in final edited form as:

ACS Chem Biol. 2015 November 20; 10(11): 2448–2454. doi:10.1021/acschembio.5b00627.

Controlled co-reconstitution of multiple membrane proteins in lipid bilayer nanodiscs using DNA as a scaffold

Thomas Raschle[1,*,4], **Chenxiang Lin**[1,2,3], **Ralf Jungmann**[1,2,3], **William M. Shih**[1,2,3], and **Gerhard Wagner**[1,*]

[1]Department of Biological Chemistry and Molecular Pharmacology, Harvard Medical School, Harvard University, Boston, MA 02115, USA

[2]Department of Cancer Biology, Dana-Farber Cancer Institute, Harvard University, Boston, MA 02115, USA

[3]Wyss Institute for Biologically Inspired Engineering, Harvard University, Boston, MA 02115, USA

Abstract

Nanodiscs constitute a tool for the solubilization of membrane proteins in a lipid bilayer, thus offering a near-native membrane environment. Many membrane proteins interact with other membrane proteins, however, the co-reconstitution of multiple membrane proteins in a single nanodisc is a random process that is adversely affected by several factors, including protein aggregation. Here, we present an approach for the controlled co-reconstitution of multiple membrane proteins in a single nanodisc. The temporary attachment of designated oligonucleotides to individual membrane proteins enables the formation of stable, detergent-solubilized membrane protein complexes by base-pairing of complementary oligonucleotide sequences, thus facilitating the insertion of the membrane protein complex into nanodiscs with defined stoichiometry and composition. As a proof of principle, nanodiscs containing a hetero-dimeric and hetero-trimeric membrane protein complex were reconstituted using fluorescently-labeled voltage-gated anion channel (VDAC) as a model system.

Membrane proteins are predicted to account for 18–29% of all encoded proteins[1] and play crucial roles in various biological functions including respiration, signal transduction and molecular transport[2]. Often, membrane proteins function as part of larger membrane protein assemblies, characterized by specific protein-protein interactions that are important for protein regulation, targeting, and activity. A recent proteome-wide study identified on average ~2.1 interactions per membrane protein[3]. Despite their importance, detailed knowledge about protein-protein interactions of integral and lipid-anchored membrane proteins is still significantly under-represented.

*Corresponding authors: Gerhard Wagner and Thomas Raschle (gerhard_wagner@hms.harvard.edu and traschle@creoptix.com).
[4]Current address: Einsiedlerstrasse 34, 8820 Wädenswil, Switzerland

ASSOCIATED CONTENT

Supporting Information

Additional experimental procedures, oligonucleotide sequences, VDAC cysteine mutant data, time-dependent fluorescence data, and equations are included in the supporting information. This material is available free of charge via the Internet at http://pubs.acs.org.

The *in vitro* characterization of membrane protein complexes by biochemical and biophysical means poses severe challenges, often requiring isolated and detergent-solubilized membrane protein complexes. However, detergent micelles might interfere with the stability of the membrane protein complex by disrupting weak or transient protein-protein associations due to the denaturing properties of the chosen detergent.

Sligar *et al*. introduced lipid bilayer nanodiscs as an alternative to the use of detergents for the solubilization of membrane proteins[4]. The absence of detergents in combination with a native-like lipid bilayer membrane environment supports both function and stability of the embedded membrane protein[5]. The nanodisc technology has greatly advanced the investigation of integral membrane proteins such as channels[6,8,10], GPCR[12,13,14] and other receptors[15,16,17], transporters[18,19,20] and membrane enzymes[21,22,23] using a multitude of different functional and structural methods. However, the currently used method for the co-reconstitution of multiple membrane proteins in a single nanodisc is often inadequate as it relies on adjusting the protein concentrations during nanodisc assembly[24,25]. The requirement for detergent-solubilized membrane protein at relatively high concentrations of at least 50 μM for efficient nanodisc formation is not always feasible for a particular membrane protein, and the removal of detergent during nanodisc assembly might favor protein aggregation over nanodisc incorporation. Furthermore, the incorporation of membrane proteins is a stochastic process, leading to nanodiscs with a random distribution of incorporated membrane proteins regarding the number of incorporated proteins[16,17] as well as their molecular composition, thus necessitating either additional steps for the isolation of the intended complex[26] or sophisticated statistical methods for analysis of the experimental data. A further level of complexity is introduced by the possibility for bi-directional insertion of the membrane protein into the lipid bilayer, further reducing the yield of correctly inserted membrane protein multimers. To address these limitations, we developed a method to provide better control over the stoichiometry and composition of the nanodisc-embedded membrane proteins during *in vitro* co-reconstitution. Our approach employs the tagging of individual detergent-solubilized membrane proteins with a short oligonucleotide (Scheme 1). The oligonucleotide encodes the protein identity as well as the information for complex formation. Transient, DNA-tethered protein complexes are formed through base pairing of complementary nucleotide sequences. The resulting high local concentration of the membrane proteins facilitates their co-incorporation into a single nanodisc during nanodisc assembly. Removal of the DNA scaffold yields the untethered membrane protein complex with the specified molecular composition in a stable lipid bilayer environment. This manuscript establishes proof of principle by demonstrating the assembly of nanodiscs containing specified heteromeric dimers and trimers of an integral polytopic membrane protein.

To assemble heterodimeric membrane protein complexes, two oligonucleotides with complementary regions at the 5’- and 3’-end were designed, forming an antiparallel duplex DNA with a central six nucleotide region without base pairing to allow for greater flexibility of the DNA scaffold (Supporting Scheme S1a). The length of the terminal portion of the oligonucleotide was optimized in order to minimize the mean distance between the attached membrane proteins for efficient incorporation into a single nanodisc, while keeping a

minimal length to guarantee sufficient stability of the DNA double strand. The architecture of the DNA-scaffold design favors the insertion of membrane proteins in a parallel orientation. The insertion of monomers from opposite sides of the nanodisc is theoretically possible, although entropically less favorable. The formation of a heterotrimer is accomplished using three different oligonucleotides, featuring two regions for complementary base pairing, whereby each oligonucleotide forms an antiparallel duplex DNA with each of the other two oligonucleotides (Supporting Scheme S1b). The VDAC protein was used as a model system to establish proof-of-principle[27]. Detergent-solubilized VDAC protein was modified with the designated oligonucleotides in separate reactions using a bifunctional crosslinker. The availability of high-resolution 3D structures facilitated a structure guided approach to identify potential sites for modification. Three different single-cysteine variants of the VDAC protein were prepared and tested for their accessibility by the crosslinker probe (Supporting Figure S1a). The single-cysteine mutant C127S, having one of two native cysteines substituted by a serine, was selected for all further experiments because of sufficient labeling efficiency and a minimal disturbance of the wildtype protein sequence. The S215C single-cysteine mutant showed a reduced labeling efficiency, while the V3C mutant showed comparable labeling efficiency. Reproducible conjugation yields of ~65% were obtained when using a two times molar excess of oligonucleotide-crosslinker probe over the protein, and a yield of ~20% after purification of the protein-oligonucleotide conjugate. The purity of the purified VDAC oligonucleotide-conjugates was estimated by SDS-PAGE analysis to be ≥ 92% (Supporting Figure S1b).

VDAC complexes were assembled by mixing equimolar amounts of the respective VDAC-oligonucleotide conjugates solubilized in detergent micelles. Formation of the DNA duplex structure by base-pairing of the complementary nucleotide sequences resulted in the appearance of higher molecular weight species as evidenced by SDS-PAGE analysis (Figure 1a and b). Protein complexes with approximately double and triple the molecular mass of the VDAC-oligonucleotide conjugate indicated DNA-tethered dimeric and trimeric VDAC complexes, respectively. Nanodiscs were assembled according to published protocols[28] using an eight times molar excess of nanodisc over VDAC protein. Nanodiscs containing His-tagged VDAC were separated from excessive empty nanodiscs and characterized by size exclusion chromatography (Figure 1c and d). The yield of nanodisc-incorporated VDAC with respect to the VDAC-oligonucleotide conjugate is approximately 5%. The elution profile of the multimeric VDAC-oligonucleotide nanodisc assemblies indicated the formation of two main species with an estimated Stokes hydrodynamic diameter of 12.5 nm and 13.6 nm for peak A and peak B, respectively. The retention volume of peak A indicates correctly assembled nanodiscs. The slightly increased Stokes hydrodynamic diameter of peak A when compared to nanodiscs assembled with un-tagged VDAC in the control reaction (Stokes hydrodynamic diameter of 12.3 nm) is likely a consequence of the attached DNA scaffold. Indeed, removal of the DNA scaffold by DNAse results in the appearance of a predominant nanodisc species with an identical retention volume as observed for nanodiscs assembled with untagged VDAC (Figure 1c and d, red and green line). SDS-PAGE analysis of the peak fraction indicated the co-elution of the respective dimeric and trimeric VDAC-oligonucleotide multimers with the membrane scaffold protein, confirming the successful incorporation of VDAC multimers into nanodiscs (Figure 1e and f).

Furthermore, treatment of the peak fraction with DNAse led to the disappearance of the band corresponding to the dimeric and trimeric VDAC multimer with the concomitant appearance of a band for unmodified VDAC. Further proof for the correct assembly of nanodiscs is provided by the imaging of negatively-stained peak fractions by transmission electron microscopy (TEM) (Figure 2). TEM imaging of peak fraction A for both $(VDAC)_2$- and $(VDAC)_3$-nanodiscs revealed correctly assembled nanodiscs[29] with a diameter of 13.0 ± 0.8 nm (N=221) and 13.1 ± 0.9 nm (N=98), respectively. Analysis of peak fraction B revealed the predominant occurrence of pairs of nanodiscs for both $(VDAC)_2$- and $(VDAC)_3$-nanodiscs. This observation can be rationalized by the DNA scaffold-mediated tethering of two individual nanodiscs each containing a single VDAC protein as illustrated in Supporting Scheme S2. This finding is in agreement with the observation of a larger Stokes diameter as observed by SEC (Figure 1c and d) and was further corroborated by the observation of singular nanodisc particles after removal of the oligonucleotide scaffold by DNAse (Figure 2). Analogous to the formation of nanodisc-dimers (Supporting Scheme S2), the tethering of three separate nanodiscs, each containing a single VDAC molecule, by the DNA-scaffold can be envisioned. TEM imaging of peak fraction C (Figure 1d) did indeed reveal nanodisc trimers as well as larger molecular weight aggregates (Supporting Figure S2b). The presence of aggregates is due to overlap with the void volume of the size exclusion column.

Encoding the identity of the protein in the nucleotide sequence of the attached oligonucleotide facilitates the incorporation of different membrane proteins with desired molecular composition in a single nanodisc. As a proof of principle, nanodiscs containing two and three copies of a distinguishable VDAC protein, *i.e.* heteromeric $(VDAC)_2$- and $(VDAC)_3$-nanodiscs, were assembled. The different VDAC-oligonucleotide conjugates were labeled with fluorescent dyes having distinct spectral properties, thus enabling to experimentally distinguish individual VDAC molecules by fluorescence microscopy. Nanodisc preparations corresponding to SEC-peak fraction A were treated with DNAse, re-purified by SEC and adsorbed to glass cover slips at concentrations low enough to provide well separated single nanodisc particles. Emitted fluorescence light was recorded after excitation of the fluorescent dyes by total internal reflection fluorescence (TIRF) (Figure 3 and Supporting Figures S3 and S4). Images were analyzed for co-localization of the attached fluorescent dyes to determine the composition of the membrane protein complex at the single nanodisc level. Assembled $(VDAC)_2$-nanodiscs displayed 47 ± 9 % co-localization (N=1758) while the control reaction for nanodiscs assembled with untagged VDAC resulted in 3 ± 3 % co-localization (N=1208). Co-reconstitution of VDAC trimers resulted in 35 ± 8 % co-localization (N=2389), while 0.2 ± 0.5 % (N=576) co-localization was observed for the control reaction. The lower than anticipated yield of co-reconstitution can be attributed to several factors, including photo-bleaching of the fluorophores as well as sub-stoichiometric fluorophore labeling of the protein resulting in an underestimation of the co-localization. The yield of co-localization is further reduced by the sub-optimal baseline separation of DNA-tethered nanodisc-dimers/-trimer and correctly assembled singular nanodiscs by SEC (Fig. 2a and b, Peak A and B). During nanodisc assembly, the contamination with VDAC-protein without oligonucleotide modification will result in the insertion of monomeric VDAC molecules, reducing the yield of co-localization. As an

example in the case of the $(VDAC)_2$-nanodisc, an estimated purity of 94.4% for the VDAC-oligonucleotide conjugate d2 (estimated by SDS-PAGE; Figure 1a and Supporting Figure S3a) will translate into a maximal theoretical yield of 89.4 % co-localization (Supporting Equation S1). Moreover, non-equimolar concentrations of the individual VDAC-conjugates present during nanodisc assembly, will also affect the yield of the desired VDAC multimer, further reducing co-reconstitution of the membrane protein complex.

In summary, the presented approach yields highly pure nanodiscs containing either a hetero-dimeric or heterotrimeric integral membrane protein complex with a 16- or 175-fold enrichment, respectively, over the control reaction. It is noteworthy that the expected yield of co-localization for un-tagged protein under the conditions used in this study, *i.e.* an eight-fold molar excess of nanodiscs over VDAC, would be 0.36% (Supporting Equation S2) and 0.01% (Supporting Equation S3) for VDAC-dimer and –trimer, respectively.

This proof-of-principle study demonstrates the use of a temporary DNA-scaffold to precisely control the composition of co-reconstituted membrane proteins in nanodiscs. The spatial constraint imposed by the boundary of the membrane scaffold protein restricts the exchange of individual membrane proteins with other nanodisc particles thus artificially stabilizing the membrane protein complex. The current protocol for the reconstitution of multiple membrane proteins into nanodiscs has several drawbacks that limit the use of nanodiscs for the investigation of membrane protein complexes. In particular, the requirement for relatively high protein concentrations for efficient nanodisc assembly, the stochastic nature of the incorporated membrane protein complexes, and the increased risk for protein aggregation at those concentrations. An approach to minimize membrane protein aggregation involves the assembly of nanodisc in presence of a large molar excess of nanodiscs over the membrane protein of interest. It is noteworthy that in the case of the human β2-adrenergic receptor a 150-fold excess of membrane scaffold protein over membrane protein was used in order to minimize protein aggregation and maximize the incorporation of functional receptor[13]. However, assembly conditions using an excess of nanodiscs will not allow the incorporation of multiple membrane proteins into a single nanodisc unless the detergent-solubilized membrane protein complex of interest exhibits high thermal stability in the chosen detergent. The approach described here enables the controlled co-reconstitution of multiple membrane proteins in presence of an excess of nanodiscs, thus limiting the potential for membrane protein aggregation during assembly. The (reversible) attachment of a designated oligonucleotide imparts the protein with the ability to temporarily assemble into a highly stable protein multimer with a defined oligomerization level and composition to facilitate co-reconstitution into nanodiscs. In addition, the DNA scaffold is expected to facilitate the co-directional insertion of the membrane proteins, thus increasing the fraction of correctly inserted subunits of a multimeric membrane protein assembly. It can be readily envisioned that the presented approach could also be of use to assemble correctly oriented membrane protein complexes in liposomes.

At this stage of method validation, a bi-functional crosslinker was used for linking protein to oligonucleotide. Future studies will explore disulfide coupling of the oligonucleotide to the protein as a reversible protein modification of cysteine residues, enabling the production of

co-reconstituted membrane protein complexes without any remaining linker moiety. It is noteworthy that the presented approach relies on the presence of a single cysteine residue that is both accessible and reactive, possibly requiring mutagenesis to either remove excess cysteine residues and/or to introduce a non-native cysteine residue into the protein sequence. As an alternative, one could also envision the site-specific introduction of a reactive un-natural amino acid for conjugation with the oligonucleotide.

The feasibility to co-reconstitute functionally coupled membrane proteins into lipid bilayer nanodiscs is expected to offer unique opportunities to probe their function and structure. G-protein coupled receptors (GPRCs) represent one example of a class of membrane proteins that are well known to be regulated through formation of homo- and heteromeric protein complexes[30]. A second important class of cell-surface receptors is the family of receptor tyrosine kinases (RTKs). The binding of growth factors to the extracellular domain of the receptor leads to receptor dimerization and activation of the intracellular tyrosine kinases domain[31]. The possibility to prepare nanodiscs containing receptor dimers in absence of ligand and to study their dimerization upon ligand binding will provide a new tool to study receptor signaling.

METHODS

Materials

The construct pET21:hVDAC1[32] was used in this study for the expression of human VDAC-1. To reduce protein flexibility, all constructs used in this study harbor the E73V mutation described by Villinger S. *et al.*[33]. Protein mutants were generated using the QuikChange site-directed mutagenesis kit (Stratagene) with pET21:hVDAC1[32] as the template. The plasmid pMSP1E3D1[29] was obtained from addgene (www.addgene.org) and used for the expression of the apolipoprotein A1 derived membrane scaffold protein (MSP1E3D1). The oligonucleotide sequences for scaffold assembly were designed using the nucleic acid package (nupack.org) software[34].

Protein preparation

Expression, purification and refolding of human VDAC-1 protein was carried out as described[35]. In addition and subsequent to the cation exchange chromatography, a size exclusion chromatography step was included. A HiLoad 16/600 Superdex 200 pg column (GE Healthcare) was equilibrated with buffer A (50 mM sodium phosphate, pH 7.5, 200 mM NaCl, 0.5 mM EDTA and 0.1% (w/v) LDAO). Pure VDAC-1 fractions were pooled and concentrated using ultrafiltration devices (Centricon MWCO 10,000; Millipore).

The expression and purification of the nanodisc protein MSP1E3D1 was done as described[36]. MSP1E3D1 without the His-tag (MSP1D1E3(−)) was prepared by incubation with TEV protease followed by retention of His-tagged TEV protease, uncleaved MSP1E3D1 and cleaved off His-tag on a Ni-chelating column. MSP1E3D1(−) was collected in the flow-through and dialyzed over-night at 4°C against buffer B (20 mM Tris-Cl, pH 7.5, 100 mM NaCl, 0.5 mM EDTA).

Oligonucleotide conjugation reaction

In a first step, the primary amine at the 5'-end of the oligonucleotide was reacted with the amine-reactive N-hydroxysuccinimide (NHS) ester moiety of the bifunctional crosslinker $SM(PEG)_4$. In a second step, the cysteine-reactive maleimide moiety of the oligonucleotide-crosslinker conjugate was reacted with the VDAC protein. The reaction product was purified by affinity-, anion-exchange, and size exclusion chromatography. The reader is referred to the Supporting Information for a detailed description of the procedure.

In vitro reconstitution of VDAC-Nanodisc assemblies

Co-reconstitution of multiple VDAC proteins with the desired stoichiometry was achieved by incubating equimolar amounts of the respective, detergent-solubilized protein-oligonucleotide conjugates for 30 min at 25°C. In a control reaction, protein-oligonucleotide conjugates were treated with DNAse (Benzonase; Novagen) prior to the reconstitution reaction. The reconstitution reaction was supplied with a stock solution of a lipid mix (50 mM DMPC:DMPG, 3:1; in 100 mM Triton X-100 and 20 mM NaPi, pH 7.5) and membrane scaffold protein without a His-tag (MSP1E3D1(−)). The molar ratio of MSP1E3D1(−) : VDAC : lipid at a final concentration of 50 μM MSP1E3D1(−) was 1 : 0.06 : 125 in buffer I (50 mM Tris-Cl, pH 7.5, 0.5 mM EDTA, 400 mM NaCl and complete protease inhibitor cocktail (Roche)). The mixture was incubated for 60 min at 25°C. Nanodisc assembly was initiated by the addition of 60% (w/v) Bio-Beads SM-2 (Bio-Rad) and incubation for 4 – 16h at 25°C while rotating.

Nanodisc purification

Assembled nanodiscs containing His-tagged VDAC protein were isolated by application to Ni-NTA resin equilibrated in buffer J (5 mM imidazole, 25 mM NaPi, pH 8, 300 mM NaCl and complete protease inhibitor cocktail) and washed with 10 column volumes of buffer J to remove empty nanodiscs. Nanodiscs containing VDAC were recovered by elution in buffer K (200 mM imidazole, 25 mM NaPi, pH 8, 300 mM NaCl). The buffer of the eluate was exchanged into buffer L (20 mM Tris-Cl, pH 7.5, 250 mM NaCl, 0.5 mM EDTA) on a size exclusion chromatography column (Superdex 200, 10/300; GE Healthcare). Peak fractions were either directly analyzed or treated with DNAse to enzymatically remove the oligonucleotides. After treatment with DNAse, samples were applied to a size exclusion chromatography column (Superdex 200, 10/300, GE Healthcare) equilibrated in buffer L before analysis.

Nanodisc imaging by transmission electron microscopy (TEM)

Samples were diluted to a final concentration of 10 nM in buffer M (10 mM Tris-Cl, pH 7.5, 50 mM NaCl) and adsorbed to glow-discharged, carbon-coated EM grids (Electron Microscopy Sciences). Samples were prepared by conventional negative staining with 0.75% (w/v) uranyl formate as described previously[36]. TEM images were acquired on a Philips CM10 electron microscope (Philips Electronics, Mahwah, NJ, USA) equipped with a tungsten filament and operated at an acceleration voltage of 100 kV. Images were recorded with a Gatan 1 × 1 k CCD camera (Gatan, Inc., Pleasanton, CA, USA) at a magnification of

52,000 and a defocus value of ~1.5 μm. Images were processed and analyzed with the program ImageJ[37].

Nanodisc imaging by fluorescence microscopy

Samples were diluted to a final concentration of 10 pM in buffer N (5 mM Tris-Cl, pH 8, 25 mM NaCl and 2.5 mM $MgCl_2$) and adsorbed to glass cover slips (Micro Cover Glasses, No. 1.5; VWR). The cover glass was sealed onto a microscope glass slide with nail polish and mounted on the sample stage with the coverslip facing towards the objective. Images were acquired on an inverted Nikon Ti-E microscope (Nikon Instruments) with integrated Perfect Focus System and equipped with a Nikon 100× 1.49 NA TIRF DIC objective lens. An additional 1.5 magnification was used to obtain a final imaging magnification of ~150 fold, corresponding to a pixel size of 107 nm. An Agilent MLC400B laser equipped with a fiber-optic delivery system was used for TIRF excitation at wavelengths of 488 nm, 561 nm and 647 nm with power levels of 50 mW, 50 mW and 125 mW, respectively. Fluorescence light was spectrally filtered with the following emission filters (Chroma Technologies); peak transmissions and bandwidths are 525/50 for Alexa Fluor 488 imaging, 600/50 for Alexa Fluor 561 imaging and 700/75 for Alexa Fluor 647 imaging. The fluorescent light was imaged on a 512×512 back-illuminated electron multiplying cooled CCD camera (Andor DU-897; Andor Technology) with the following acquisition parameters; acquisition time 100 – 300 ms, a read-out rate of 5 MHz at 14-bit, a EM gain multiplier of 256 and a 5× conversion gain. The laser was operated at a power level of 32% (488 TIRF), 19% (561 TIRF) and 10% (647 TIRF) of the maximal power. The microscope was operated with the NIS-Elements image acquisition software (Nikon).

Image processing

The TIRF images were processed using ImageJ[37]. The percentage of co-localization was quantified using an ImageJ script.

Supplementary Material

Refer to Web version on PubMed Central for supplementary material.

Acknowledgments

This research was supported by NIH grants GM075879 (to G. Wagner). We thank the Nikon Imaging Center at Harvard Medical School and the molecular electron microscopy facility (NIH grant PO1 GM62580 to S. C. Harrison) for the use of their microscopes. We would like to thank M. Chambers and T. Walz (Harvard Medical School) for help with electron microscopy.

REFERENCES

1. Kihara D, Kanehisa M. Tandem clusters of membrane proteins in complete genome sequences. Genome Res. 2000; 10:731–743. [PubMed: 10854407]
2. Arinaminpathy Y, Khurana E, Engelman DM, Gerstein MB. Computational analysis of membrane proteins: the largest class of drug targets. Drug Discov Today. 2009; 14:1130–1135. [PubMed: 19733256]
3. Babu M, Vlasblom J, Pu S, Guo X, Graham C, Bean BDM, Burston HE, Vizeacoumar FJ, Snider J, Phanse S, Fong V, Tam YYC, Davey M, Hnatshak O, Bajaj N, Chandran S, Punna T, Christopolous

C, Wong V, Yu A, Zhong G, Li J, Stagljar I, Conibear E, Wodak SJ, Emili A, Greenblatt JF. Interaction landscape of membrane-protein complexes in Saccharomyces cerevisiae. Nature. 2012; 489:585–589. [PubMed: 22940862]

4. Bayburt TH, Sligar SG. Membrane protein assembly into Nanodiscs. FEBS Lett. 2010; 584:1721–1727. [PubMed: 19836392]
5. Etzkorn M, Raschle T, Hagn F, Gelev V, Rice AJ, Walz T, Wagner G. Cell-free expressed bacteriorhodopsin in different soluble membrane mimetics: Biophysical properties and NMR accessibility. Structure. 2013; 21:394–401. [PubMed: 23415558]
6. Katayama H, Wang J, Tama F, Chollet L, Gogol EP, Collier RJ, Fisher MT. Three-dimensional structure of the anthrax toxin pore inserted into lipid nanodiscs and lipid vesicles. Proc. Natl. Acad. SciUSA. 2010; 107:3453–3457.
7. Raschle T, Hiller S, Yu T-Y, Rice AJ, Walz T, Wagner G. Structural and functional characterization of the integral membrane protein VDAC-1 in lipid bilayer nanodiscs. J. Am. Chem. Soc. 2009; 131:17777–17779. [PubMed: 19916553]
8. Hagn F, Etzkorn M, Raschle T, Wagner G. Optimized phospholipid bilayer nanodiscs facilitate high-resolution structure determination of membrane proteins. J. Am. Chem. Soc. 2013; 135:1919–1925. [PubMed: 23294159]
9. Etzkorn M, Raschle T, Hagn F, Gelev V, Rice AJ, Walz T, Wagner G. Cell-free expressed bacteriorhodopsin in different soluble membrane mimetics: biophysical properties and NMR accessibility. Structure. 2013; 21:394–401. [PubMed: 23415558]
10. Alami M, Dalal K, Lelj-Garolla B, Sligar SG, Duong F. Nanodiscs unravel the interaction between the SecYEG channel and its cytosolic partner SecA. EMBO J. 2007; 26:1995–2004. [PubMed: 17396152]
11. Mitra N, Liu Y, Liu J, Serebryany E, Mooney V, Devree BT, Sunahara RK, Yan ECY. Calcium-dependent ligand binding and g-protein signaling of family B GPCR parathyroid hormone 1 receptor purified in nanodiscs. ACS Chem. Biol. 2013; 8:617–625. [PubMed: 23237450]
12. Whorton MR, Bokoch MP, Rasmussen SGF, Huang B, Zare RN, Kobilka B, Sunahara RK. A monomeric G protein-coupled receptor isolated in a high-density lipoprotein particle efficiently activates its G protein. Proc. Natl. Acad. SciUSA. 2007; 104:7682–7687.
13. Leitz AJ, Bayburt TH, Barnakov AN, Springer BA, Sligar SG. Functional reconstitution of β2-adrenergic receptors utilizing self-assembling Nanodisc technology. Biotechniques. 2006; 40:601–612. [PubMed: 16708760]
14. Inagaki S, Ghirlando R, White JF, Gvozdenovic-Jeremic J, Northup JK, Grisshammer R. Modulation of the interaction between neurotensin receptor NTS1 and Gq protein by lipid. J. Mol. Biol. 2012; 417:95–111. [PubMed: 22306739]
15. Zocher M, Roos C, Wegmann S, Bosshart PD, Dotsch V, Bernhard F, Muller DJ. Single-molecule force spectroscopy from nanodiscs: An assay to quantify folding, stability, and interactions of native membrane proteins. ACS Nano. 2012; 6:961–971. [PubMed: 22196235]
16. Boldog T, Grimme S, Li M, Sligar SG, Hazelbauer GL. Nanodiscs separate chemoreceptor oligomeric states and reveal their signaling properties. Proc. Natl. Acad. SciUSA. 2006; 103:11509–11514.
17. Shi L, Shen Q-T, Kiel A, Wang J, Wang H-W, Melia TJ, Rothman JE, Pincet F. SNARE Proteins: One to Fuse and Three to Keep the Nascent Fusion Pore Open. Science. 2012; 335:1355–1359. [PubMed: 22422984]
18. Dalal K, Chan CS, Sligar SG, Duong F. Two copies of the SecY channel and acidic lipids are necessary to activate the SecA translocation ATPase. Proc. Natl. Acad. Sci. 2012
19. Alvarez FJD, Orelle C, Davidson AL. Functional reconstitution of an ABC transporter in nanodiscs for use in electron paramagnetic resonance spectroscopy. J. Am. Chem. Soc. 2010; 132:9513–9515. [PubMed: 20578693]
20. Frauenfeld J, Gumbart J, van der Sluis EO, Funes S, Gartmann M, Beatrix B, Mielke T, Berninghausen O, Becker T, Schulten K, Beckmann R. Cryo-EM structure of the ribosome-SecYE complex in the membrane environment. Nat. Struct. Mol. Biol. 2011; 18:614–621. [PubMed: 21499241]

21. Mazhab-Jafari MT, Marshall CB, Stathopulos PB, Kobashigawa Y, Stambolic V, Kay LE, Inagaki F, Ikura M. Membrane-dependent modulation of the mTOR activator Rheb: NMR observations of a GTPase tethered to a lipid-bilayer nanodisc. J. Am. Chem. Soc. 2013; 135:3367–3370. [PubMed: 23409921]
22. Luthra A, Gregory M, Grinkova YV, Denisov IG, Sligar SG. Nanodiscs in the studies of membrane-bound cytochrome P450 enzymes. Methods Mol. Biol. 2013; 987:115–127. [PubMed: 23475672]
23. Nasvik Ojemyr L, Von Ballmoos C, Gennis RB, Sligar SG, Brzezinski P. Reconstitution of respiratory oxidases in membrane nanodiscs for investigation of proton-coupled electron transfer. FEBS Lett. 2012
24. D'Antona AM, Xie G, Sligar SG, Oprian DD. Assembly of an activated rhodopsin-transducin complex in nanoscale lipid bilayers. Biochemistry. 2014; 53:127–134. [PubMed: 24328127]
25. Bayburt TH, Grinkova YV, Sligar SG. Assembly of single bacteriorhodopsin trimers in bilayer nanodiscs. Arch. Biochem. Biophys. 2006; 450:215–222. [PubMed: 16620766]
26. Bayburt TH, Leitz AJ, Xie G, Oprian DD, Sligar SG. Transducin activation by nanoscale lipid bilayers containing one and two rhodopsins. J. Biol. Chem. 2007; 282:14875–14881. [PubMed: 17395586]
27. Colombini M. VDAC structure, selectivity, and dynamics. Biochim. Biophys. Acta - Biomembr. 2012; 1818:1457–1465.
28. Ritchie TK, Grinkova YV, Bayburt TH, Denisov IG, Zolnerciks JK, Atkins WM, Sligar SG. Chapter 11 Reconstitution of Membrane Proteins in Phospholipid Bilayer Nanodiscs. Methods Enzymol. 2009; 464:211–231. [PubMed: 19903557]
29. Denisov IG, Grinkova YV, Lazarides AA, Sligar SG. Directed Self-Assembly of Monodisperse Phospholipid Bilayer Nanodiscs with Controlled Size. J. Am. Chem. Soc. 2004; 126:3477–3487. [PubMed: 15025475]
30. Maeda S, Schertler GFX. Production of GPCR and GPCR complexes for structure determination. Curr. Opin. Struct. Biol. 2013; 23:381–392. [PubMed: 23707225]
31. Lemmon MA, Schlessinger J. Cell signaling by receptor tyrosine kinases. Cell. 2010; 141:1117–1134. [PubMed: 20602996]
32. Malia TJ, Wagner G. NMR structural investigation of the mitochondrial outer membrane protein VDAC and its interaction with antiapoptotic Bcl-XL. Biochemistry. 2007; 46:514–525. [PubMed: 17209561]
33. Villinger S, Briones R, Giller K, Zachariae U, Lange A, de Groot BL, Griesinger C, Becker S, Zweckstetter M. Functional dynamics in the voltage-dependent anion channel. Proc. Natl. Acad. SciUSA. 2010; 107:22546–22551.
34. Zadeh JN, Steenberg CD, Bois JS, Wolfe BR, Pierce MB, Khan AR, Dirks RM, Pierce NA. NUPACK: Analysis and design of nucleic acid systems. J. Comput. Chem. 2011; 32:170–173. [PubMed: 20645303]
35. Hiller S, Garces RG, Malia TJ, Orekhov VY, Colombini M, Wagner G. Solution structure of the integral human membrane protein VDAC-1 in detergent micelles. Science. 2008; 321:1206–1210. [PubMed: 18755977]
36. Raschle T, Hiller S, Yu T-YYTY, Rice AJAAJ, Walz T, Wagner G. Structural and functional characterization of the integral membrane protein VDAC-1 in lipid bilayer nanodiscs. J Am Chem Soc. 2009; 131:17777–17779. [PubMed: 19916553]
37. Schneider CA, Rasband WS, Eliceiri KW. NIH Image to ImageJ: 25 years of image analysis. Nat. Methods. 2012; 9:671–675. [PubMed: 22930834]

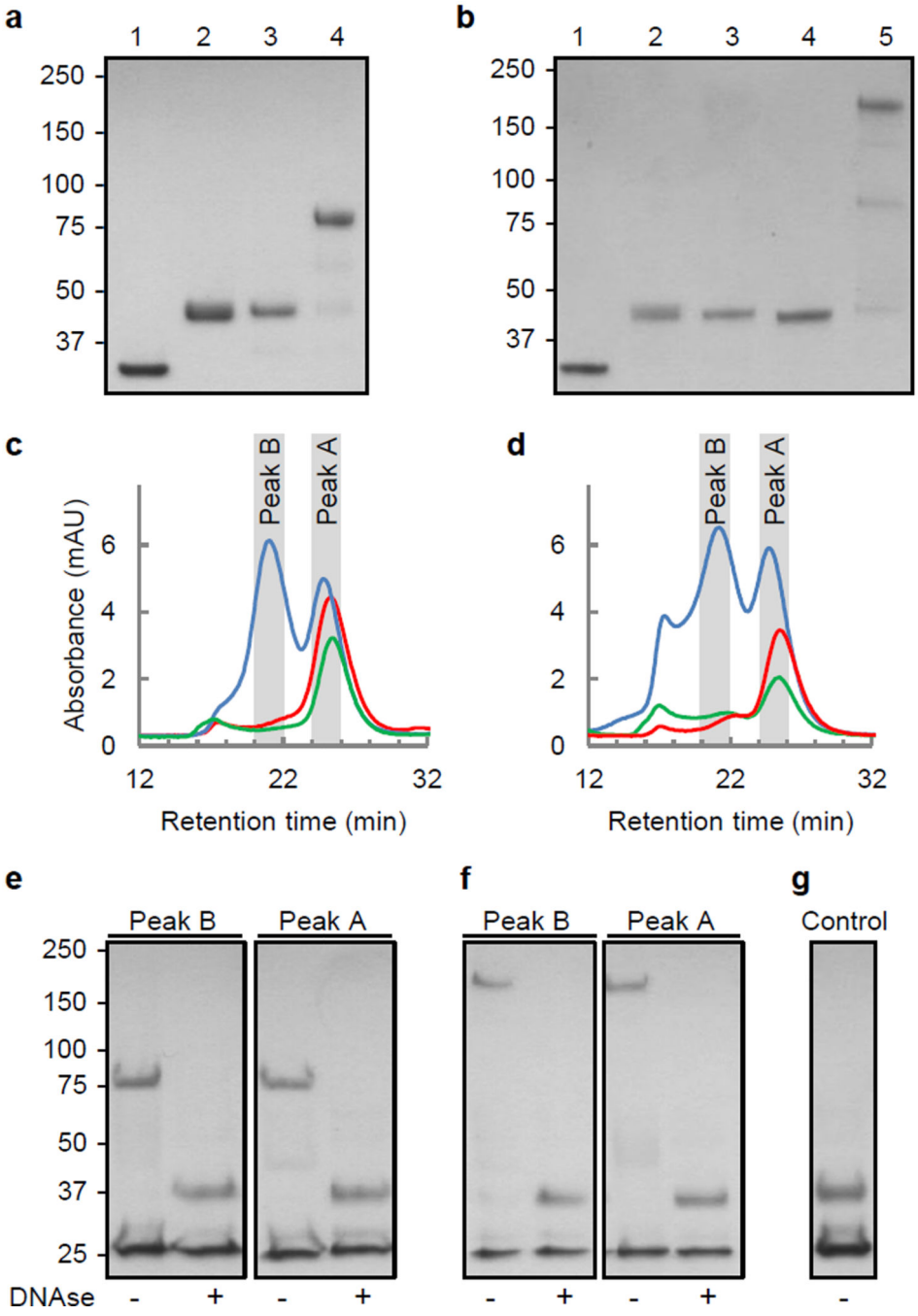

Figure 1.

Characterization of dimeric and trimeric VDAC multimers in detergent and nanodiscs. (a) DNA-tethered VDAC dimer in detergent micelles. Lane 1, unmodified VDAC; lane 2–3, VDAC-oligonucleotide-t1 and -d2 conjugate; lane 4, equimolar mixture of the VDAC-oligonucleotide conjugates from lane 2 and lane 3; (b) DNA-tethered VDAC trimer in detergent micelles. Lane 1, unmodified VDAC; lane 2–4, VDAC-oligonucleotide-t1, -t2 and -t3 conjugates; lane 5, equimolar mixture of VDAC-oligonucleotide conjugates from lanes 2–4. For a list of molecular masses see Supporting Table S1. Size exclusion

chromatographic (SEC) analysis of $(VDAC)_2$- (c) and $(VDAC)_3$-nanodiscs (d) before (blue) and after (green) removal of the DNA scaffold. Nanodiscs assembled with un-tagged VDAC in a control reaction are shown in red. SDS-PAGE analysis of the SEC peak fractions of the $(VDAC)_2$- (e) and $(VDAC)_3$-nanodiscs (f) before and after treatment with DNAse. The control reaction (g) shows the SEC peak fraction of nanodiscs assembled with un-tagged VDAC.

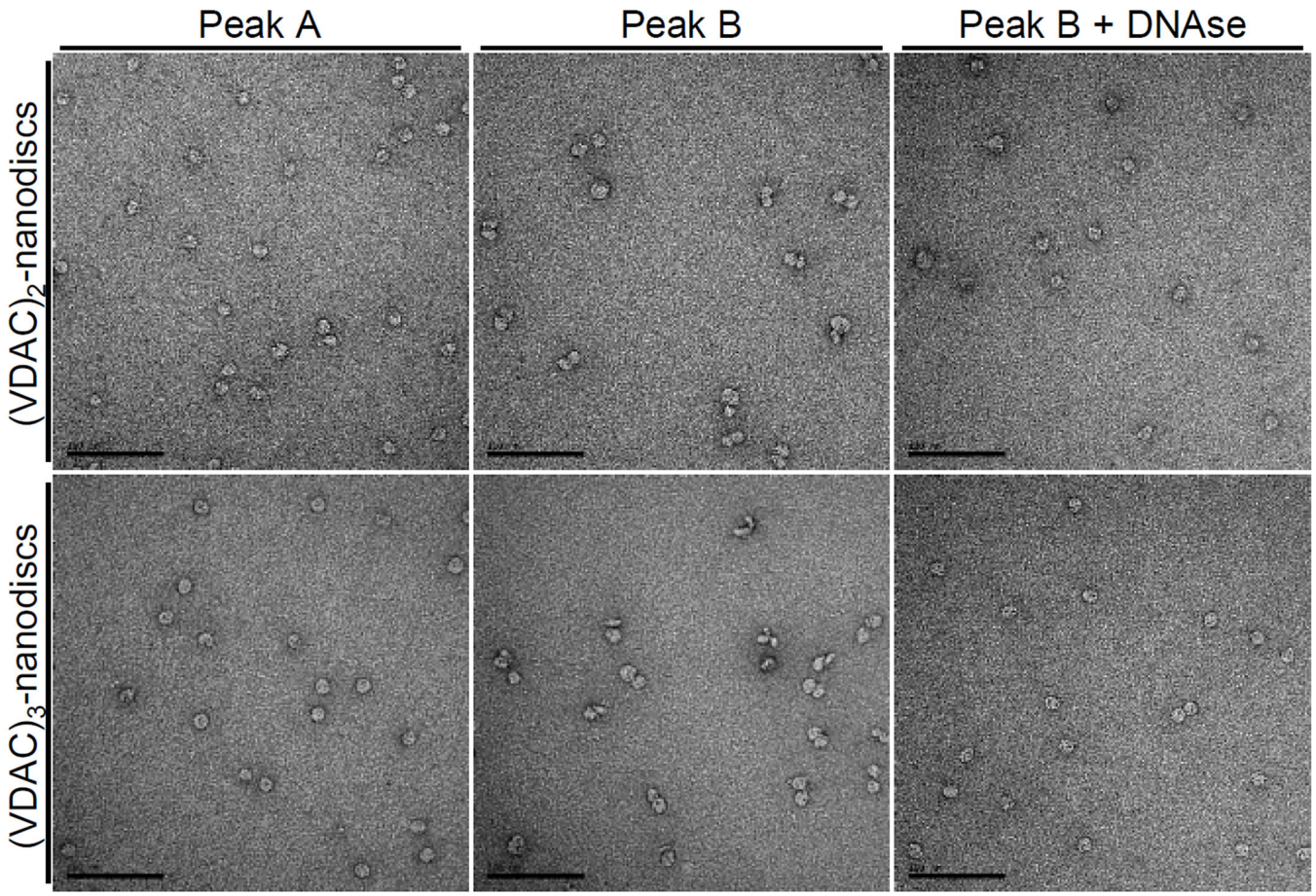

Figure 2.

Characterization of VDAC-nanodiscs by negative stain transmission electron microscopy. Representative images of SEC peak fractions for $(VDAC)_2$- and $(VDAC)_3$-nanodiscs before and after treatment with DNAse. A representative TEM image of the SEC peak fraction of empty nanodiscs as well as peak fraction C is shown in Supporting Figure S2. The scale bar is 100 nm.

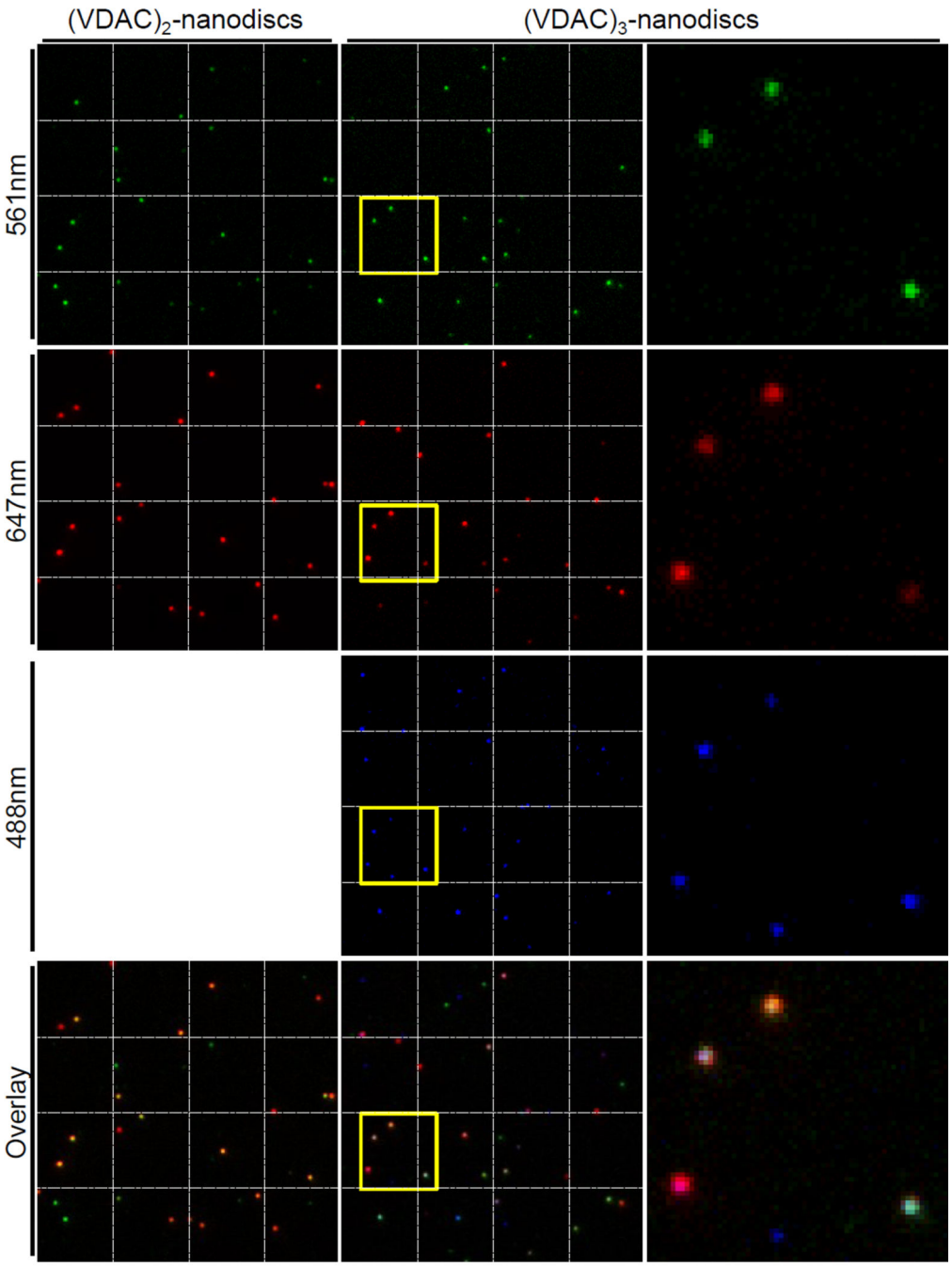

Figure 3.

Single molecule analysis of nanodisc particles by fluorescence microscopy. Representative TIRF images of $(VDAC)_2$- and $(VDAC)_3$-nanodiscs. Nanodiscs assembled with un-tagged VDAC (control) are shown in Supporting Figure S5. Emitted fluorescent light was recorded from the same field of view after excitation at the wavelength specified. An overlay is shown at the bottom. The area indicated with a yellow box is shown enlarged in the row on the right (dimensions 6.8 × 6.8 μm). The images have dimensions of 27.3 × 27.3 μm.

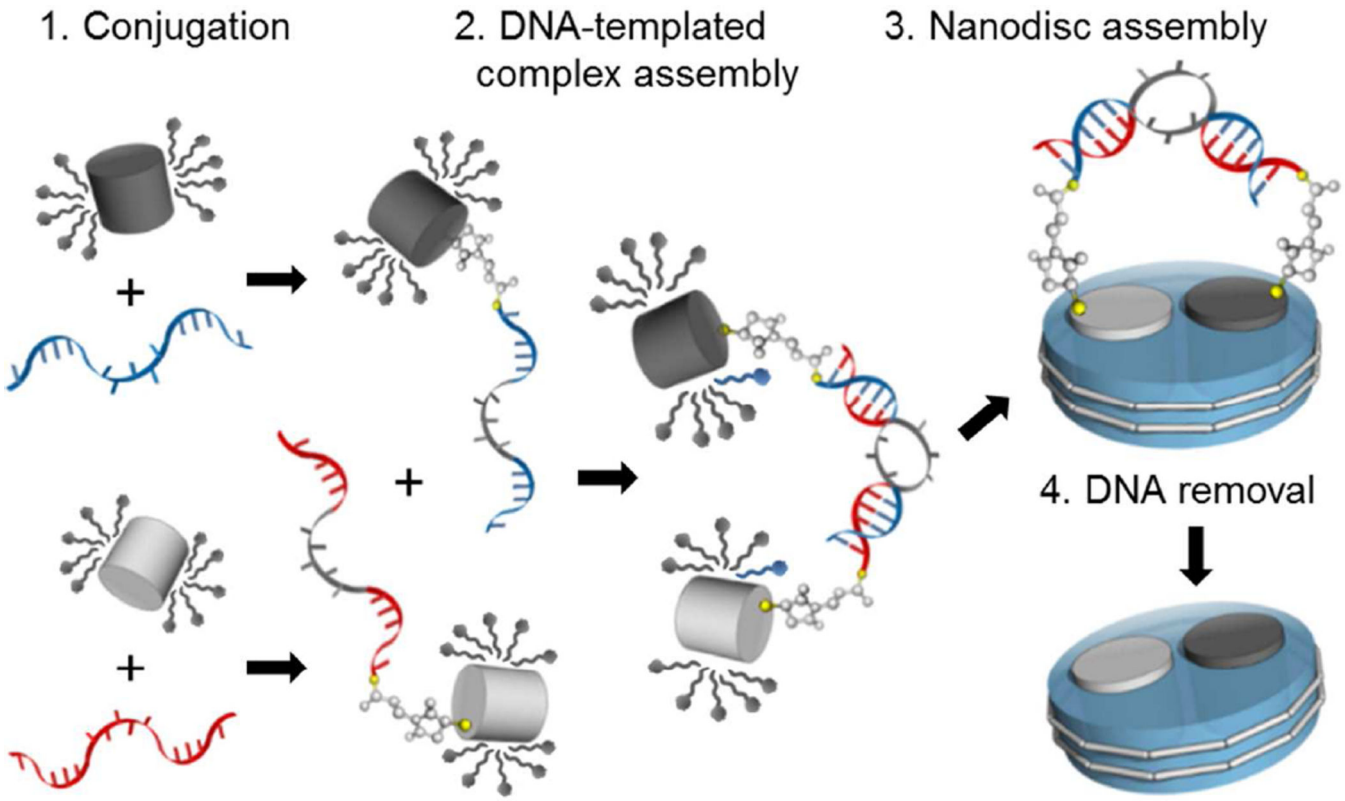

Scheme 1.
DNA-scaffold approach for the directed assembly of membrane protein complexes.